ORIGINAL ARTICLE

lajss.org Latin American Journal of Solids and Structures

www.lajss.org

Damage Laws of Large-Sized Multimedium Materials by Shaped Charge Jets

Yipu Dou[a], Zhengfeng Liang[a], Jianhao Dou[a*]

[a]Xi'an Modern Chemistry Research Institute, Xi'an 710065, China. Email: dou_yp@qq.com, 2042lzf@sohu.com, 504080702@qq.com

*Corresponding author

https://doi.org/10.1590/1679-7825/e8386

Abstract

During penetration into large-sized multimedium materials, shaped charge jets are affected by jet fracture and interface effect, leading to reductions in their penetration performance. A theoretical model and calculation method for the penetration of shaped charge jets into asphalt/soil/concrete composite targets were established and experimentally verified to explore the law of the jet-induced damage of large-sized multimedium materials. The influence of the shaped waves generated during the penetration of shaped charge jets, jet fracture, and the interface effect at the interface between different media on the penetration performance of shaped charge jets were taken into account. The theoretical calculation results are in good agreement with the test results. In addition, through dimensional analysis and theoretical calculation, the curve chart of the relationship between total penetration depth and asphalt/soil part thickness is obtained. This chart can quickly reflect the law of the penetration of shaped charges into media with differing thicknesses.

Keywords

shaped charge jet, large-sized target, multimedium, interface effect

Graphical Abstract

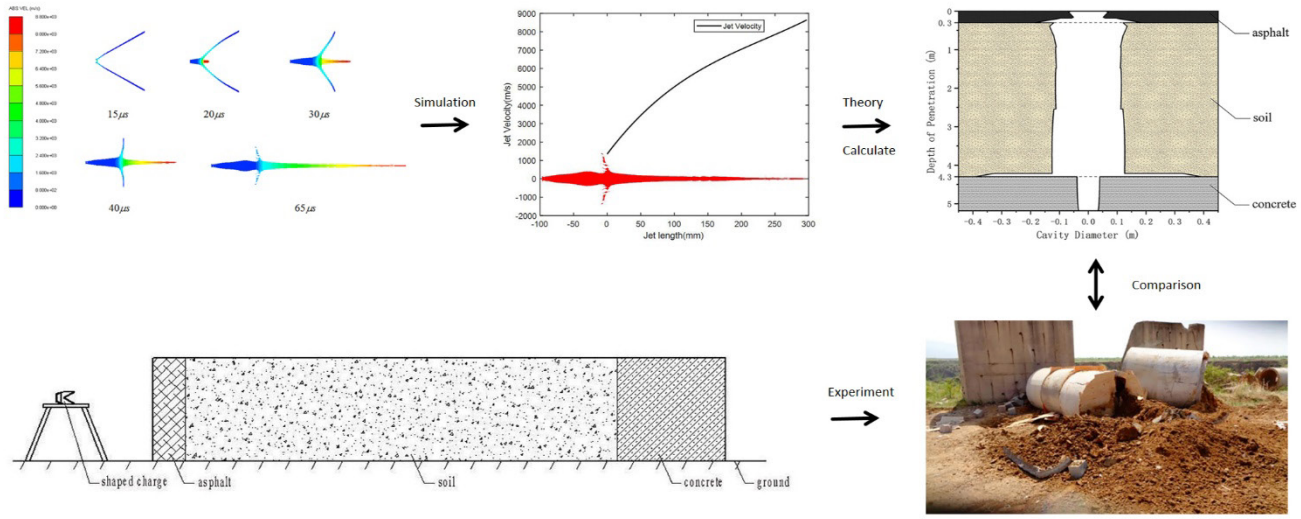

Received: September 28, 2024. In revised form January 14, 2025. Accepted January 22, 2025. Available online: January 24, 2025.
https://doi.org/10.1590/1679-7825/e8386

Latin American Journal of Solids and Structures. ISSN 1679-7825. Copyright © 2025. This is an Open Access article distributed under the terms of the Creative Commons Attribution License, which permits unrestricted use, distribution, and reproduction in any medium, provided the original work is properly cited.

1 INTRODUCTION

In modern warfare, the battlefield has transformed from field operations to urban warfare, and the destruction of underground construction has become an important goal (Li et al. 2019). Shaped charge jets, which are a common means of attacking armored targets, have been generally used to attack fortification-type targets with large wall thicknesses by virtue of their great penetration depth. Targets, such as underground buildings in cities, are often located under soil several meters thick. The surface of the soil layer is also covered with asphalt. This asphalt/soil/concrete structure is a large-sized multimedium material structure. It has been widely used in underground shopping malls, subways, and airport runways. Furthermore, shaped charge jets are frequently employed in the perforation procedures within the domain of oil and gas exploitation, with the aim of establishing conduits between the wellbore and hydrocarbon reservoirs (Liu, J. et al. 2019, Liu, X. B. et al. 2023). These jets are required to penetrate through the casing, cement sheath, and geological formations. In the event of complex geological circumstances, the formations may encompass a variety of rock strata. Consequently, the investigation into the penetration regularities of shaped charge jets within large-sized multimedium materials can render the application of shaped charges in engineering practice more efficacious and reliable. Shaped charge jets are more prone to fracture when penetrating into large-sized targets than when penetrating into armored homogeneous targets, and the penetration speed of jets is affected by the reflection of penetration-induced shock waves at the interface between two media, thus influencing the penetration performance of jets. Therefore, in this study, the laws of the penetration of shaped charge jets into large-sized multimedium materials were investigated with an asphalt/soil/concrete composite medium target as an example.

Penetration depth and penetration hole diameter are the main parameters used to describe the penetration performance of shaped charge jets. Many researchers have deeply explored the theoretical models of jet penetration. Chen and Li (2002) analyzed the expanding model of a dynamic cavity and proposed a formula for predicting penetration depth in soil or concrete. Szendrei (1983, 1995) obtained an equation for calculating penetration hole diameter. Held (1995, 1996, 1999) corrected and experimentally verified this equation. When penetrating into large-sized single-medium materials, shaped charge jets usually experience fracture, and the fractured jet segments are subjected to drift and rotation, resulting in a decline in their penetration depth and an increase in their penetration hole diameter. Chou (1977, 1986) analyzed the influence of the particle gap of fractured jets on penetration depth and posited that the penetration depth of the fractured jets decreases with the increase in particle gap. Segletes (1983) studied the influence on the drift velocity of jet particles by X-ray and discovered that drift velocity increases with the increase in jet velocity. Held (1983) came to the opposite conclusion, believing that drift velocity declines due to the acceleration of jet velocity. Shelton and Arbuckle (1979) calculated the maximum particle size after the copper jet was broken. In contrast to when they penetrate large-sized single-medium materials, shaped charge jets are affected by the interface effect between adjacent media when they penetrate large-sized multimedium materials. When the initial velocity of the jet head is greater than the sound velocity of the target, shock waves are generated during jet penetration into the target. When propagating into the interface of two media, shock waves are reflected and transmitted, forming reflected and transmitted waves, respectively, which affect penetration depth. Xiao et al. (2013, 2017, 2020) analyzed the influence of plastic waves generated during the penetration of shaped charge jets into a soil–concrete composite target. Church, Cornish and Cullis (2001) conducted numerical simulations and experiments on the penetration of shaped charge jets into concrete, sand, soil, and multimedium targets. In addition, some scholars have analyzed, tested, and numerically simulated the penetration of shaped charge jets into multilayer targets (Mamivand et al. 2010, Jia et al. 2013, 2014, Zu et al. 2015).

Although many scholars have studied the penetration of jets into single-medium targets, the penetration of shaped charge jets into large-sized multimedium targets has been rarely investigated. Composite targets are divided into different parts for calculation in accordance with different media. This step is followed by simple addition. However, this approach fails to consider the influence of jet fracture and the interface effect. In this study, on the basis of jet PER and one-dimensional hydrodynamic penetration theories and in consideration of the impact of shock wave reflection at the interface of different media, a theoretical model of the penetration of shaped charge jets into asphalt/soil/concrete composite targets was established, and a calculation method for the penetration depth of jets in concrete layers under the known thickness of asphalt and soil was obtained. Next, the penetration of shaped charge jets into asphalt/soil/concrete was experimentally investigated, and the above models were verified. In addition, the curve chart of the relationship between the total penetration depth of shaped charges and thickness of asphalt/soil parts was obtained through dimensional analysis on the basis of the theoretical calculation model. Furthermore, the laws underlying the jet-induced damage of media differing in thicknesses were analyzed. This study will be an important reference for designing shaped charge warheads that destroy composite media.

In this study, several variables are defined and utilized. Since the jet model is divided into a finite number of microelements for analysis, the subscript *i* will be appended to certain variables, which stands for the corresponding variable of the ith microelement of the jet. For instance, v_j is used to denote the jet velocity, while v_{ji} indicates the velocity of the ith infinitesimal element of the jet. Moreover, the target is composed of three components, namely asphalt, soil and concrete. In certain circumstances, the subscript *i* can represent a specific number. For instance, in the expression v_{j1}, it represents the velocity of the first jet microelement.

2 Theory analysis

The process of jet penetration into a target can be partitioned into three distinct phases. In the initial phase of penetration, shock waves are induced, leading to the rupture of the free surface of the target plate accompanied by debris ejection. A region characterized by high temperature, high pressure, and high strain rate is established, which merely constitutes a negligible fraction of the overall penetration depth. Subsequently, the stable penetration stage ensues. Within this stage, the energy of the jet varies at a sluggish pace, and the associated penetration parameters remain relatively invariant. The preponderance of the depth of the penetration hole is generated during this period. Eventually, upon the exhaustion of the high-velocity segment of the jet, if the jet velocity falls below the critical penetration velocity of the target, further penetration becomes infeasible. Alternatively, the jet may experience fracture, precipitating a rapid deterioration in its penetration performance. The residual jet debris accumulates at the base of the penetration hole, thereby culminating the penetration process.

Birkhoff (1948) analyzed the problem of jet penetration based on the one-dimensional hydrodynamic theory. Assuming that both the target and the jet are ideal, incompressible, and inviscid fluids, the penetration equation of the jet can be derived without considering the strength of the target:

$$\frac{1}{2}\rho_j(v_j-u)^2=\frac{1}{2}\rho_t u^2 \tag{1}$$

Where ρ_j and ρ_t are the jet and target densities, respectively; v_j is velocity of jet, u is penetration velocity. This formula does not describe the impact of shock waves generated during the penetration process and the effect of jet fracture.

When a shaped charge jet begins to penetrate into a target, its penetration produces shock waves because its velocity is considerably faster than the sound velocity of the target. The parameters of the target material change after the generation of shock waves, which affect jet penetration performance. During penetration, jet velocity gradually decreases, and shock waves are not induced by penetration when jet velocity is less than a certain value.

Fractures would occur when the jet is sufficiently elongated. Jet segments after fracture are subjected to flipping and drifting, and pits must be re-excavated for penetration, leading to the substantial degradation of penetration performance.

In accordance with the above analysis and in consideration of the effect of shock waves and jet fractures on penetration, the following assumptions were made on the basis of jet PER and one-dimensional hydrodynamic penetration theories:

(1) Metal jet velocity is linearly distributed.

(2) Asphalt, soil, and concrete are all ideal elastic–plastic materials of homogenous isotropy.

(3) The lateral dimension of the target is infinitely large. Therefore, it is unaffected by the boundary effect during penetration, and the influence of unloading waves is not considered.

(4) After jet fracture, each jet segment undergoes rotation and drift, but velocity and diameter no longer change.

(5) Generally, the attenuation of stress waves can be described as an exponential function or power function (Leong et al. 2007, Yankelevsky et al. 2011, Zhang et al. 2020). In this study, the attenuation of stress waves in the target was described via an exponential function.

(6) The target parameters before and after shock waves are strongly discontinuous and change instantly.

2.1 A sub-section Penetration of a shaped charge jet

A jet is divided into a finite number of microelements. Assume that the jet consumed at each fixed time step Δt is regarded as one jet microelement, and the distance between the first element and the target is L_0. The time t_i when the ith jet microelement starts to penetrate is

$$t_i=\frac{L_0}{v_{j1}}+\Delta t(i-1) \tag{2}$$

where v_{j1} is velocity of the first jet microelement. When the velocity of a jet microelement is higher than a specific limit, this microelement generates shock waves during penetration, changing the target status near the projectile–target interface (Xiao et al. 2013). Bernoulli's equation can be listed as follows in accordance with the target status after shock waves:

$$\frac{1}{2}\rho_j(v_{ji}-u_i)^2=\frac{1}{2}\rho_t u_i^2+\frac{1}{2\lambda}\rho_t u_i(u_i-C_t)+R_t \tag{3}$$

where v_{ji} is velocity of the ith jet microelement; u_i is penetration velocity of the ith jet microelement; C_t is the sound velocity of the target; R_t is the target resistance; and λ is a constant, the value of λ ranges from 1.5 to 2.2 (Grady 1996), the value of λ is set to be 1.7 in the calculation. By calculating this equation, the penetration velocity of the ith microelement can be solved as

$$u_i=\frac{(2\lambda\rho_j v_{ji}-\rho_t C_t)-\sqrt{4\lambda\rho_j\rho_t v_{ji}((1+\lambda)v_{ji}-C_t)+8\lambda R_t(\lambda\rho_j-(1+\lambda)\rho_t)+\rho_t^2C_t^2}}{2\lambda\rho_j-2(1+\lambda)\rho_t},\ v_{ji}>C_t+\sqrt{\frac{\rho_t C_t^2}{\rho_j}+\frac{2R_t}{\rho_j}} \tag{4}$$

As the velocity of the penetrating jet microelement gradually declines, no shock wave is produced during penetration. Bernoulli's equation and penetration velocity in this case are described as

$$\frac{1}{2}\rho_j(v_{ji}-u_i)^2=\frac{1}{2}\rho_t u_i^2+R_t \tag{5}$$

$$u_i=\frac{v_{ji}-\sqrt{\frac{\rho_t}{\rho_j}v_{ji}^2+(1-\frac{\rho_t}{\rho_j})\frac{2R_t}{\rho_j}}}{1-\frac{\rho_t}{\rho_j}},\ v_{ji}\le C_t+\sqrt{\frac{\rho_t C_t^2}{\rho_j}+\frac{2R_t}{\rho_j}} \tag{6}$$

The penetration depth P_i of the ith jet microelement in the target is

$$P_i=u_i\Delta t \tag{7}$$

Given the velocity gradient in the jet, the jet continuously elongates until fracture after formation. Following jet fracture, the velocity, length, and diameter of each jet segment no longer change, whereas the fractured jet segment is subjected to radial drift, reversal, and fly-off, resulting in a considerable decline in penetration performance.

According to the study conducted by Zheng (1981), jet fracture time is correlated with jet diameter and velocity gradient. The fracture time t_{bi} of the ith jet microelement is expressed as

$$t_{bi}=c_b(d_{0i}^2\frac{dl}{dv})^{\frac{1}{3}} \tag{8}$$

where c_b is a constant associated with the jet material, d_{0i} is the diameter of the ith jet microelement, and dl/dv is the reciprocal of the jet velocity gradient. Before t_{bi}, during the continuous stretching process of the jet, the diameter of the jet microelement decreases, while its volume remains unchanges and its length increases. The ith jet microelement is in a fractured state after t_{bi}, and both its length and diameter cease to change. The diameter of the ith jet microelement after fracture is

$$d_{bi}=d_{0i}\sqrt{\frac{1}{\frac{dv}{dl}t_{bi}+1}} \tag{9}$$

where d_{bi} is the diameter upon the fracture of the ith jet microelement. After the jet fractures, the fractured jet segments undergo radial drift and form an axial spacing with the adjacent jet segment. If the ith jet microelement is in a fractured state before it starts to penetrate, the skew distance δ_i (Xiao et al. 2015) and microelement spacing g are

$$\delta_i=C_1 v_{ji}t_i+C_2\frac{d_{bi}}{t_{bi}}(t_i-t_{bi}) \tag{10}$$

$$g=(v_{ji-1}-v_{ji})(t_i-t_{bi}) \tag{11}$$

where C_1 and C_2 are constants and can be divided into two circumstances in accordance with the charge status:

Precise charge: C_1 = 0 and C_2 = 0.24.

Non-precise charge: C_1 = 0.0028 and C_2 = 0.24.

Given that the penetration performance of the fractured jet microelement is affected, Equation (7) must be corrected (Xiao et al. 2015):

$$P_i = u_i t[1 - (\frac{2\delta_i}{D_{ci}-d_{bi}})^{1.5}](1 - 0.2e^{-\frac{2d_{bi}}{g}}) \tag{12}$$

where D_{ci} is the penetration crater diameter, When the velocity of the jet microelement is less than the critical penetration velocity of the target or the jet microelement is exhausted, penetration stops, and the sum of the penetration depths formed by all jet microelements completing penetration is the penetration depth of the whole jet into the composite target, namely,

$$P = \sum_1^i P_i \tag{13}$$

After the ith microelement completes penetration, when the head of the $i+1^{th}$ microelement operates to the jet–target interface, the operation distance is equivalent to the sum of the penetration depth P that has already been achieved, the distance S_{i+1} between the $i+1^{th}$ microelement and the first microelement in the initial state, and the distance L_0 between the first microelement and the target. Therefore, the velocity of the $i+1^{th}$ microelement is

$$v_{ji+1} = \frac{\sum_1^i P_i + S_{i+1} + L_0}{t_{i+1}} \tag{14}$$

2.2 Influence of the interface effect

The shock waves generated during jet penetration affect the state of the target, resulting in changes in the density, impedance, and particle velocity of the target. Equation (4) is the calculation formula for the penetration velocity in this case. The reflected waves formed when the shock waves travel to the surface of the composite medium contribute to the secondary change in the target status, thus affecting the penetration performance of the jet.

The pressure generated when the first jet microelement collides with the target, which is also the initial strength p_0 of the shock waves, can be calculated in accordance with Bernoulli's principle. The initial velocity u_{s0} of the shock waves can be calculated as follows (Xiao et al. 2013, Meyers 1994):

$$p_0 = \frac{1}{2}\rho_j(v_{j1} - u_1)^2 \tag{15}$$

$$u_{s0} = \frac{C_t}{2}(1 + \sqrt{\frac{4V\lambda p_0}{C_t^2}}) \tag{16}$$

where u_1 is the penetration velocity of the first jet microelement, V is the specific volume of the target material, namely, $1/\rho_t$.

During the propagation of the shock waves, the peak value attenuates exponentially, and the attenuation equation is (Xiao 2017)

$$p_x = p_0 e^{-\gamma x} \tag{17}$$

where γ is attenuation coefficient of compaction wave and x represents the propagation distance of the shock waves.

Given the penetration of the jet, the energy of the shock waves is continuously supplemented. Hence, the velocity of the shock waves is assumed to remain equal to the penetration velocity after attenuating to a value equal to the penetration velocity. During the subsequent penetration process, the shock waves first propagate to the asphalt/soil interface, forming reflected waves. The peak value of the reflected waves at the interface and particle velocity behind the reflected wave are calculated as (Xiao 2017)

$$\frac{p_R}{p_I} = \frac{\rho_{t1}C_{t1} - \rho_{t2}C_{t2}}{\rho_{t1}C_{t1} + \rho_{t2}C_{t2}} \tag{18a}$$

$$\frac{v_R}{v_I} = \frac{\rho_{t2}C_{t2} - \rho_{t1}C_{t1}}{\rho_{t1}C_{t1} + \rho_{t2}C_{t2}} \tag{18b}$$

where p_I is the strength of the shock waves, p_R is the strength of the reflected waves, v_I represents the particle velocity behind the shock waves, and v_R is the particle velocity behind the reflected waves, ρ_{t1} and C_{t1} represent the density and wave velocity of the material in front of the interface respectively, ρ_{t2} and C_{t2} represent the density and wave velocity of the material behind the interface respectively. The relationship between the wave velocity of the reflected wave u_R and the particle velocity behind the wave v_R is

$$u_R = C_t + \lambda v_R \tag{19}$$

The velocity direction of the reflected waves is opposite the penetration velocity. Therefore, the propagation of the reflected waves in the target is not supplemented, and its peak value is continuously attenuated in accordance with Formula (17). When the jet passes through the reflected waves, the status of the target is changed by the reflected waves. In this case, the Bernoulli and penetration velocity calculation equations are

$$\frac{1}{2}\rho_j(v_j - u_i)^2 = \frac{1}{2}\rho_R(u_i - v_R)^2 + R_R \tag{20}$$

$$u_i = \frac{(1-\frac{\rho_R v_R}{\rho_j v_j})v_j - \sqrt{[(1-\frac{\rho_R v_R}{\rho_j v_j})^2 - 1 + \frac{\rho_R}{\rho_j}]v_j^2 + (1-\frac{\rho_R}{\rho_j})\frac{\rho_R}{\rho_j}v_R^2 + (1-\frac{\rho_R}{\rho_j})\frac{2R_R}{\rho_j}}}{1-\frac{\rho_R}{\rho_j}} \tag{21}$$

where ρ_R and R_R represent the density and resistance of the target behind the reflected wave respectively.

3 Test and analysis

3.1 Experimental part

An experiment was performed on shaped charge jets penetrating into asphalt/soil/concrete composite targets by using shaped charges with diameters of ϕ148 and ϕ120 mm to verify the correctness of the theoretical model. For shaped charges, the explosive used was Octol, the liner was made of copper, and the stand-off was 700 mm. The two types of shaped charge structures were similar, as shown in Figure 1.

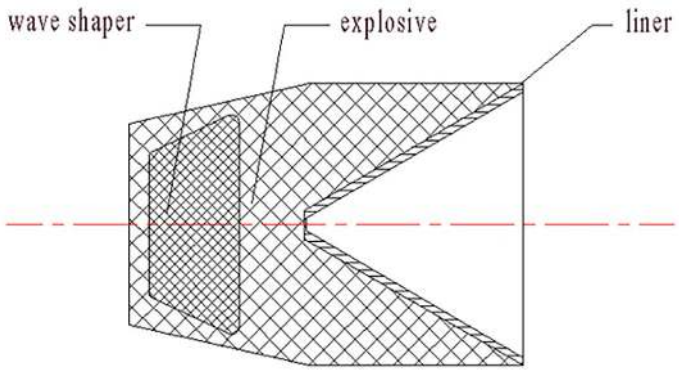

Figure 1 Shaped charge structure.

Usually, the penetration depth of shaped charges with spacers into 45-steel is 7–9 times the charge diameter. In accordance with the density law, the penetration depths of the ϕ148 and 120 mm shaped charges in the target with soil as the single medium were estimated to be approximately 5–6 and 4–5 m, respectively. Therefore, the thicknesses of the asphalt, soil, and concrete parts were set to 0.3, 4, and 0.75 m, respectively. The test conditions are listed in Table 1, and the schematic of the test device is shown in Figure 2.

Table 1 Experimental conditions.

Charge diameter (mm)	Stand-off (mm)	Target thickness (m)		
		Asphalt	Soil	Concrete
148	700	0.3	4	0.75
120	700	0.3	4	0.45

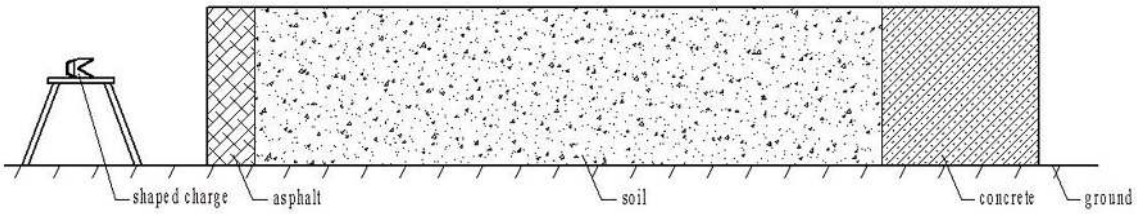

Figure 2 Schematic of the experimental device.

During target construction, an asphalt block with a 0.4 m × 0.4 m cross-section and thickness of 0.3 m was used as the asphalt part of the composite target. A cement pipe 1 m in diameter and 1 m in length was filled with soil and compacted, and multiple cement pipes filled with soil were held horizontally and axially aligned as the soil part of the composite target. For the purpose of ensuring that the state of the soil in the experiment is as proximate as possible to that of the original soil, the characteristic parameters of the soil were measured, specifically encompassing unit weight, moisture content, cohesion as well as internal friction angle. The parameters of both the original soil and the soil utilized in the experiment are presented in Table 2. Compared with original soil, the unit weight of the test soil decreased by 0.9%, the moisture content decreased by 9.56%, the cohesion decreased by 7.27%, and the internal friction angle increased by 7.06%. The differences in physical and mechanical properties between the original soil and the soil in the experiment are relatively small. Moreover, standard C40 concrete blocks with a side length of 150 mm were stacked to form the concrete part of the composite target. The concrete blocks were numbered, as shown in Figure 3, to facilitate the observation of penetration depth. Soil was piled up to an appropriate height before and behind cement pipes, ensuring that the midpoints of the asphalt, soil, and concrete parts were on the same axis. A concrete wall 0.5 m in thickness was set behind the composite target to guarantee test safety and prevent the jet from flying continuously after completely penetrating into the composite target plate. The test site layout is displayed in Figure 4.

Table 2 Comparison of soil parameters between the experimental soil and the original soil.

state	unit weight (kN/m^3)	moisture content (%)	Cohesion (KPa)	internal friction angle (°)
original	17.71	8.26	38.23	27.89
experimental	17.55	7.47	35.45	29.86

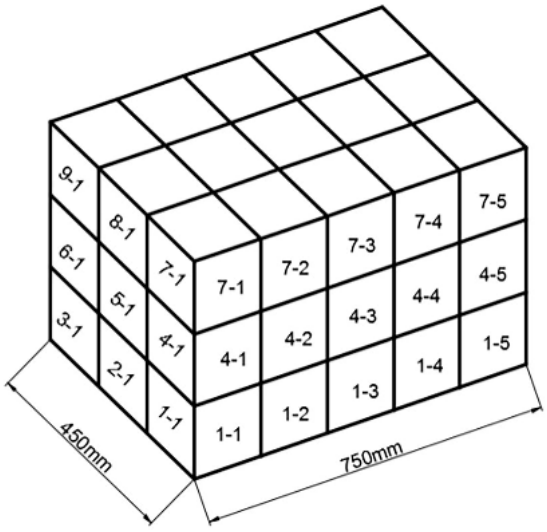

Figure 3 Numbering of concrete blocks.



a. φ148 mm *b. φ120 mm*

Figure 4 Experimental device for the penetration of shaped charges into asphalt/soil/concrete composite targets.

In the test, the asphalt part was completely broken, and the ϕ148 mm shaped charge jet continued to penetrate into the 0.675 m concrete part after penetrating through the asphalt and soil parts. The first cement pipe was broken, and concrete blocks No.4-4 and ahead were broken. The ϕ120 mm shaped charge jet penetrated into asphalt and soil but not into concrete. The test results are listed in Table 3, and the targets by jet penetration are shown in Figure 5 and Figure 6.

Table 3 Experimental results.

Charge diameter (mm)	Soil inlet cavity diameter (mm)	Soil outlet cavity diameter (mm)	Penetration depth (m)		
			Asphalt	Soil	Concrete
148	230 × 200 (at 1.3 m)	ϕ180	0.3	4	0.675
120	250 × 200	ϕ150	0.3	4	0



a. *b.*

Figure 5 Penetration effect of the ϕ148 mm shaped charge jet on the asphalt/soil/concrete composite target.



a. *b.*

Figure 6 Penetration effect of the ϕ120 mm shaped charge jet on the asphalt/soil/concrete composite target.

In the case of a short penetration distance, the jet velocity was fast, the elongation degree was small, and the energy per unit length was high such that the asphalt and soil located in the front had high kinetic energies of radial diffusion. Accordingly, a large penetration hole diameter can form, and the wooden frame for fixing the asphalt and the cement pipe located at the front splattered outward after being spread. In addition, the soil in the asphalt part and front end was close to the shaped charge and more influenced by the detonation wave and products than other parts. Therefore, the asphalt part and cement pipe at the front end broke instead of forming penetration holes.

3.1 Analysis and calculation

The test conditions were analyzed and calculated by using the theoretical model. The charges of two calibers were calculated. Jet formation by shaped charges was calculated by using numerical simulation software to acquire characteristic parameters, such as jet velocity and shape. Specifically, the formation of shaped charge jets was numerically simulated by using the simulation software AUTODYN. The simulation model is displayed in Figure 7. The shaped charge structures, dimensions, and other parameters in the simulation were identical to those in the experiment.

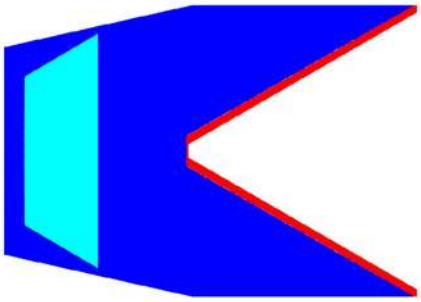

Figure 7 Simulation model.

The explosion was OCTOL, with its state equation being a JWL equation (Elshenawy et al. 2018, Baudin et al. 2010, Lee et al. 1968), as follows:

$$p = a(1 - \frac{\omega}{r_1 V})e^{-r_1 V} + b(1 - \frac{\omega}{r_2 V})e^{-r_2 V} + \frac{\omega E}{V} \tag{22}$$

where V is the specific volume; a, b, r_1, r_2, and ω are all constants; and E is the specific internal energy within unit mass. The above parameters can be found in the built-in material database of AUTODYN and are listed in Table 4.

Table 4 Explosive material parameters.

Property	Octol
Reference density (g/cm^3)	1.821
Parameter a (kPa)	7.486×10^8
Parameter b (kPa)	1.338×10^7
Parameter R_1	4.5
Parameter R_2	1.2
Parameter w	0.38
C-J Detonation velocity (m/s)	8480
C-J Energy/unit volume (kJ/m^3)	9.6×10^6
C-J Pressure (kPa)	3.42×10^7

The material of the liner was CU-OFHC, with the shock equation as its state equation and the Steinberg Guinan model as its strength model (Burakovsky et al. 2006, Guinan et al. 1975).

$$G_{GS}(p) = G_0 + (\frac{dG}{dP})_0 \frac{p}{[\eta(p)]^{1/3}} \tag{23}$$

where G is the shear modulus of the material; η is the coefficient of compressibility, and $\eta \equiv V_0/V$; and p represents pressure. The performance parameters of the purple copper shaped charge cover are exhibited in Table 5.

Table 5 Material parameters of the liner.

Parameter	CU-OFHC
Equation of state	Shock
Reference density (g/cm^3)	8.93
Gruneisen coefficient	2.02
Parameter c_0 (m/s)	3940
Parameter s	1.489
Reference temperature (K)	300
Strength model	Steinberg Guinan
Shear modulus (MPa)	4.77×10^4
Yield strength (MPa)	120
Maximum yield strength (MPa)	640

The formation of the shaped charge jet by the ϕ148 mm shaped charge liner is displayed in Figure 8. At 65 μs after detonation, the jet had already formed, and the jet segment had a total length of 297.46 mm, head velocity of 8577.5 m/s, tail velocity of 1089.1 m/s, head diameter of 1.6 mm, and tail diameter of 21.2 mm. The jet velocities corresponding to different jet positions are given in Figure 9.

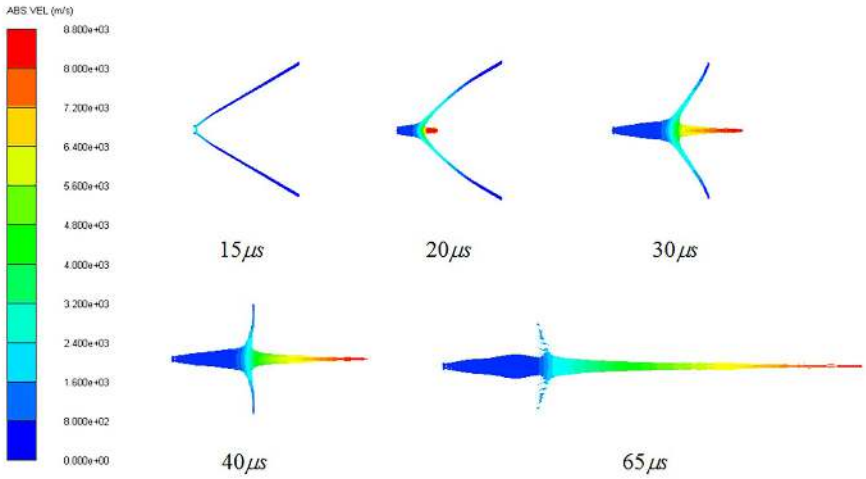

Figure 8 Formation of a shaped charge jet.

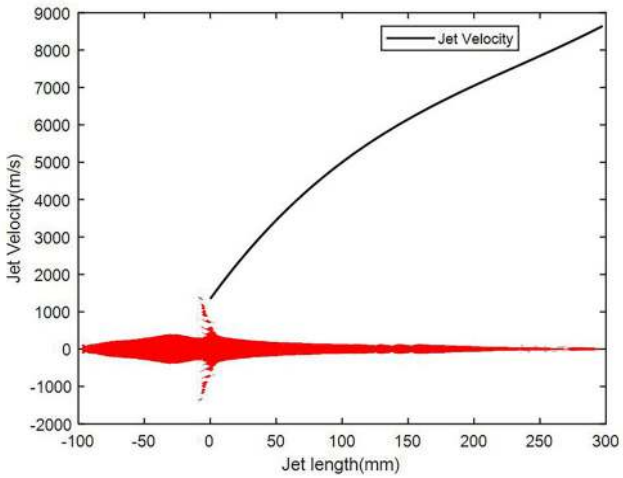

Figure 9 Jet parameters.

The penetration of the jets formed by the ϕ148 mm and ϕ120 mm shaped charges into the asphalt/soil/concrete target was calculated on the basis of the theory and the simulation results presented in this section. The material

parameters of asphalt, soil, and concrete are listed in Table 6 (Chen et al. 2013, Lu et al. 2009). The penetration velocity curve and penetration cavity diameter curve of the ϕ148 mm shaped charge are displayed in Figure 10 and Figure 11, respectively. The penetration velocity curve and penetration cavity diameter curve of the ϕ120 mm shaped charge are exhibited in Figure 12 and Figure 13, respectively.

Table 6 Target material parameters.

Parameter	Asphalt	Soil	Concrete
Length (m)	0.3	4	0.75
Density (g/cm^3)	1.2	1.79	2.45
Sound speed (m/s)	2540	200	4200
Resistance (MPa)	5	2.3	68

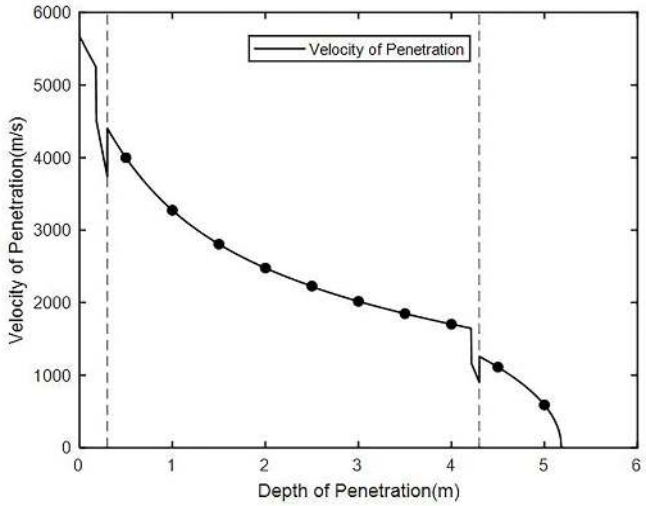

Figure 10 Penetration velocity curve of the ϕ148 mm charge.

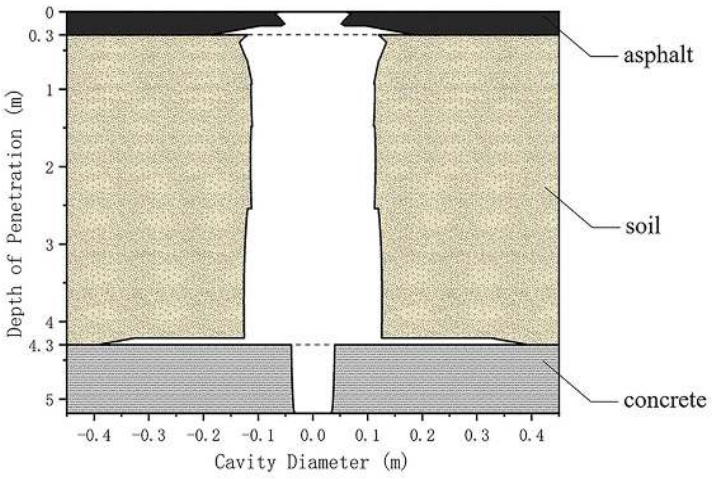

Figure 11 Penetration cavity diameter curve of the ϕ148 mm shaped charge.

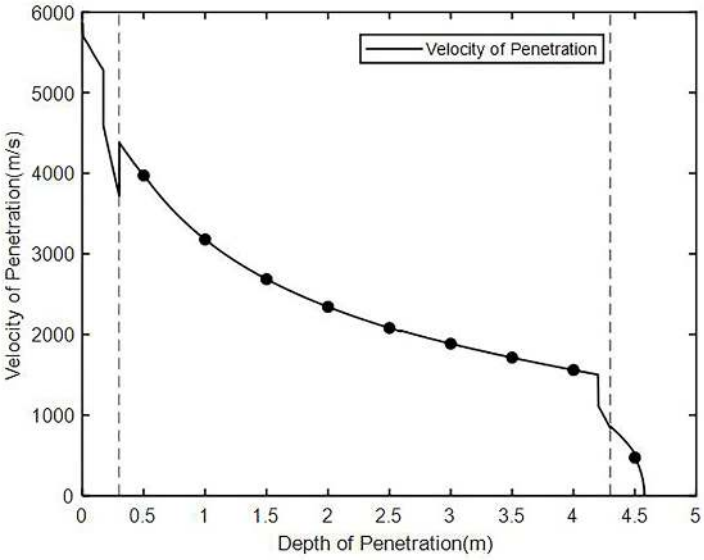

Figure 12 Penetration velocity curve of the ϕ120 mm shaped charge.

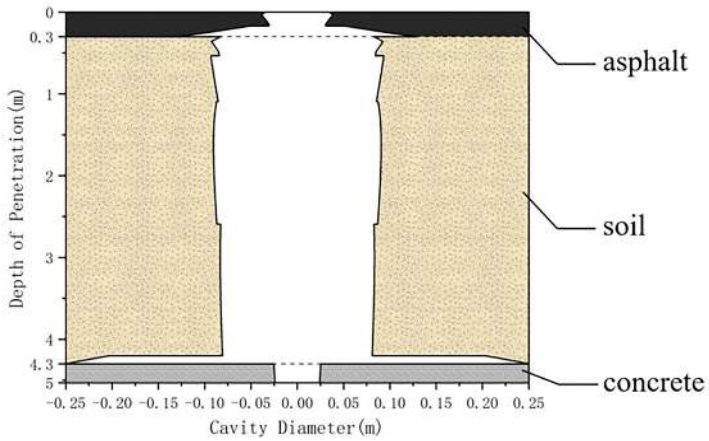

Figure 13 Penetration cavity diameter curve of the ϕ120 mm shaped charge.

According to the calculation, the jet formed by the ϕ148 mm shaped charge penetrated into 0.3 m of asphalt and 4 m of soil then continued to penetrate into 0.882 m of concrete for the total penetration length of 5.182 m. After penetrating into 0.3 m of asphalt and 4 m of soil, the jet formed by the ϕ120 mm shaped charge continued to penetrate into 0.277 m of concrete for the total penetration length of 4.577 m.

During penetration into the asphalt and soil parts, the jet velocity was high, exceeding the critical condition for shock wave formation. During penetration, shock waves were generated, and a plastic zone formed near the projectile–target interface. When the projectile–target interface was close to the interface between two media, penetration velocity declined due to the reflected waves that had formed at the interface, and the reflected waves were gradually exhausted and could not be supplemented when propagating from the interface between two media toward the projectile–target interface. Therefore, the closer the projectile-target interface to the interface between two media, the greater the influence on the penetration velocity until the jet started penetrating into the next medium. Figure 10 illustrates that the penetration velocity decreased greatly but by a small proportion under the action of the reflected waves that had formed at the asphalt/soil interface. Compared with asphalt, soil has greater density but considerably lower sound velocity such that its wave impedance is also smaller. The reflected waves that formed at the asphalt/soil interface were rarefaction waves, and the particle velocity direction behind the waves was identical to the penetration direction, exerting a small effect on penetration velocity. The reflected waves that had formed at the soil/concrete interface were compression waves, and the particle velocity direction behind the waves was opposite the penetration direction, thus exerting a great effect on penetration velocity.

The shaped charge jet fractured when penetrating into soil. The cavity diameter affected the degree to which fracture weakened jet penetration performance, whereas penetration cavity diameter was influenced by the yield strength of the

target material. The density and yield strength of soil were relatively low, and the diameter of the hole formed by penetration can reach over 10 times that of the jet. During penetration into soil, therefore, the influence of jet fracture was unnoticeable. During the stage of the penetration of the shaped charge jet into concrete, the yield strength of concrete was high. Therefore, after entering the stage of penetration into concrete, the penetration cavity diameter reduced, and the influence of jet fracture increased, accompanied with the accelerated decline in penetration velocity.

The comparison between the test and calculated results is listed in the figure 14. The total penetration depth of the ϕ148 mm shaped charge obtained in the experiment was 4.975 m, and the calculated total penetration depth was 5.182 m, indicating an error of 4.2%. The total penetration depth of the ϕ120 mm shaped charge obtained in the experiment was 4.3 m, and the calculated total penetration depth was 4.577 m, indicating an error of 6.4%. Both errors fell within the acceptable range.

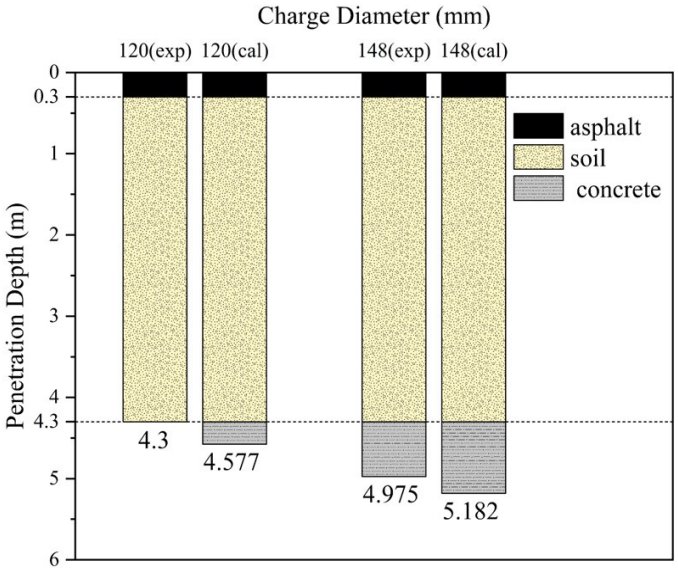

Figure 14 Comparison between experimental and calculated results.

The errors were mainly caused by the following aspects:

(1) In the test, when the shaped charge jet penetrated into soil, the cement pipe at the front end exploded, indicating that the soil part was constrained by the cement pipe. This condition resulted in a lower penetration velocity and smaller penetration hole diameter than the conditions without boundary constraints. Nevertheless, a small penetration hole diameter would amplify the impact of jet fracture and further reduce penetration velocity. Consequently, the tested penetration depth was lower than the theoretical penetration depth.

(2) Although the shaped charge used in the test had the same structure, dimensions, and materials as that used in the simulation, it had specific errors in manufacturing, assembly, and charge. As a result, the initial head velocity of the jet in the test was lower than the theoretical velocity; the drift distance was greater than the theoretical drift distance; and finally, the tested penetration depth was smaller than the theoretical penetration depth.

4 Discussion

The tests and calculations revealed that when the shaped charge jet penetrated the asphalt/soil/concrete composite target, the head velocity and drift degree upon the completion of jet penetration into the soil part greatly influenced the subsequent jet penetration performance in concrete. After the thickness of the asphalt/soil part reached a specific value, the drift degree would be excessively high after the jet penetrated through the soil part, making it impossible for the jet to penetrate into the concrete part. Hence, the total penetration depth was greatly affected by the thickness of each medium in the composite medium target. The influencing laws of the thickness of each medium in the composite target on the penetration depth of the shaped charge jet were subjected to engineering calculation and experimental studies based on the theoretical model and simulation results to further explore the laws governing the damage to large-sized multimedium materials induced by shaped charge jets.

When the explosive type and target material were fixed, the variables affecting the total penetration depth of the shaped charge jet in the asphalt/soil/concrete composite target included the charge diameter D, charge height B, explosive quantity Q, jet density ρ_j, stand-off H, material density ρ_t, sound velocity C_t, target resistance R_t, and thickness

(L_1, L_2, L_3) of each part of the target. Total penetration depth was assumed to meet functional relationships with the above variables, the functional relationship can be expressed as

$$P = f_1(D, Q, C_t, B, \rho_j, H, \rho_t, R_t, L_1, L_2, L_3) \tag{24}$$

The basic dimensions involved in the above physical quantities are length *L*, mass *M*, and time *T*. The above physical quantities are expressed by dimensions as

$$\begin{array}{c} \\ L \\ M \\ T \end{array} \begin{array}{c} \begin{array}{cccccccccccc} P & D & Q & C_t & \rho_j & H & \rho_t & B & R_t & L_1 & L_2 & L_3 \end{array} \\ \begin{bmatrix} 1 & 1 & 0 & 1 & -3 & 1 & -3 & 1 & -1 & 1 & 1 & 1 \\ 0 & 0 & 1 & 0 & 1 & 0 & 1 & 0 & 1 & 0 & 0 & 0 \\ 0 & 0 & 0 & -1 & 0 & 0 & 0 & 0 & -2 & 0 & 0 & 0 \end{bmatrix} \end{array} \tag{25}$$

Three basic dimensions, *D*, *Q*, and C_t were selected as basic physical quantities. Subsequently, these basic quantities were used to measure other physical quantities and obtain dimensionless pure numbers, which meet the following functional relationship:

$$\frac{P}{D} = f_1\left(1,1,1,\frac{B}{D},\frac{\rho_j D^3}{Q},\frac{H}{D},\frac{\rho_t D^3}{Q},\frac{R_t D^3}{Q C_t^2},\frac{L_1}{D},\frac{L_2}{D},\frac{L_3}{D}\right) \tag{26}$$

In accordance with Π theorem (Tan 2005), the left side of the above equation is a dimensionless dependent variable, whereas the coefficients of *D*, *Q*, and C_t in the right-side function f_1 are all constantly 1, having no effect on the dependent variable. The last four variables are dimensionless dependent variables that can exert effects. Therefore, Equation (23) was rewritten into the following form:

$$\frac{P}{D} = f_1\left(\frac{B}{D},\frac{\rho_j D^3}{Q},\frac{H}{D},\frac{\rho_t D^3}{Q},\frac{R_t D^3}{C_t^2 Q},\frac{L_1}{D},\frac{L_2}{D},\frac{L_3}{D}\right) \tag{27}$$

The influence of the medium thickness of each part of the large-sized multimedium target on the total penetration depth was explored as described in this section. Therefore, the stand-off, density of the jet, and performance parameters of each material part in the target could be considered to be fixed, and the charge height *B* and explosive quantity *Q* met the following functional relationships with the charge diameter.

$$B = f_2(D) \tag{28a}$$

$$Q = f_3(D, B) \tag{28b}$$

Hence, the independent variables are L_1/D, L_2/D, and L_3/D, and the dependent variable is *P*/*D*.

The influence of dimensionless variables on the penetration depth of the shaped charge jet was analyzed through the single variable method. Given that L_1/D, L_2/D, and L_3/D change simultaneously in case of a change in *D*, a fixed value was selected for the charge diameter *D*, namely, *D* = 148 mm. Under actual conditions, the thickness of the asphalt part in the asphalt/soil/concrete structure is generally less than 0.3 m, whereas that of the soil and concrete parts is unfixed (Li et al. 2023). Therefore, the asphalt thickness L_1 was set to 0, 0.1, 0.2, and 0.3 m with L_1/D = 0, 0.7, 1.4, and 2.0, respectively, and the soil thickness L_2 was set to 0, 1, 2, 3, 4, and 5 m, with L_2/D = 0, 6.8, 13.5, 20.3, 27.0 33.8, respectively. Under the above conditions, the corresponding penetration depth *P* was calculated, as listed in Table 7. P/L_2-dependent changes in *P*/*D* under different P/L_1 values are displayed in Figure 15.

Figure 15 shows that when the asphalt/soil thickness was 0 or small value, the slope of the curve remained nearly unchanged with the increase in soil thickness. After the soil thickness reached a certain value, the influence of jet fracture on jet penetration into concrete gradually intensified, and the penetration thickness in concrete decreased at an accelerated speed with the increase in the soil thickness. The calculation results revealed that when the asphalt thickness was 0.3 m, the critical thickness of soil that the 148 mm shaped charge could penetrate was 5.047 m.

The test was conducted again after adjusting the thickness of each part in the experimental target, to verify the correctness of the above theory. The new target thicknesses are listed in Table 8.

Table 7 Relationships of penetration depth with the changes in the thickness of asphalt and soil.

$L_{1/D}$ = 0		$L_{1/D}$ = 0.7		$L_{1/D}$ = 1.4		$L_{1/D}$ = 2.0	
$L_{2/D}$	P/D	$L_{2/D}$	P/D	L_2/D	P/D	L_2/D	P/D
0	25.1	0	24.8	0	25.0	0	25.2
6.8	26.9	6.8	27.0	6.8	27.2	6.8	27.2
13.5	30.1	13.5	30.1	13.5	30.4	13.5	30.1
20.3	32.6	20.3	32.7	20.3	33.0	20.3	33.1
27.0	34.3	27.0	34.5	27.0	34.7	27.0	35.0
33.8	35.7	33.8	35.9	33.8	36.2	33.8	36.6

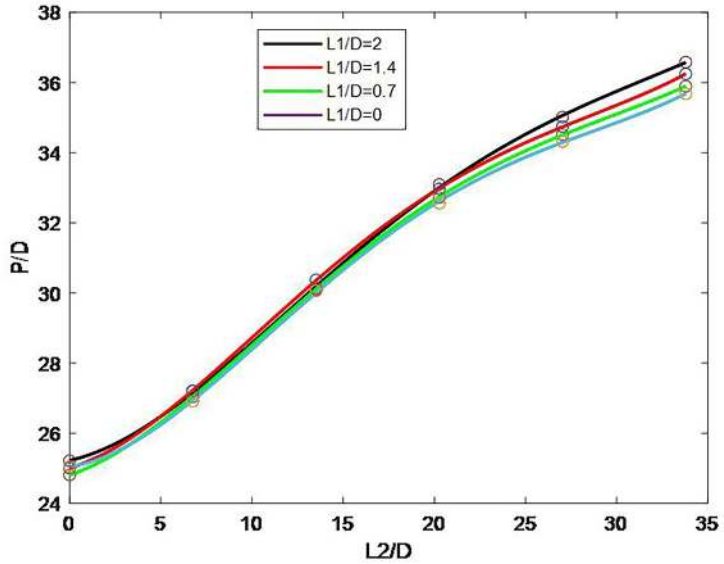

Figure 15 Relationships of total penetration depth with the changes in the thickness of different media.

Table 8 Experimental conditions for target with changed size.

Charge diameter (mm)	Stand-off (mm)	Target thickness (m)		
		Asphalt	Soil	Concrete
148	700	0.3	5	0.5
120	700	0.3	3	0.75

In the first group of tests, the ϕ148 mm shaped charge was used, the thickness of the asphalt part was kept constant at 0.3 m and that of the soil part was set to 5 m. The soil part was directly connected to the concrete wall to observe the penetration of the jet into concrete after running through soil clearly. According to the test results, the shaped charge jet penetrated through soil, leaving a pit with a diameter of 5 cm and depth of 1.5 cm in the concrete wall. The test site layout and results are shown in Figure 16.



a. experimental condition b. experimental result

Figure 16 Experimental conditions and result with the ϕ148 mm shaped charge.

In the second group of tests, the ϕ120 mm shaped charge was adopted, asphalt thickness was kept at 0.3 m, soil thickness was set to 3 m, and concrete thickness was set to 0.75 m. The test results showed that after penetrating through the soil part, the jet continued to penetrate into 0.6 m of concrete. The test site layout and test results are exhibited in Figure 17.



a. experimental condition *b. experimental result*

Figure 17 Experimental condition and result with the ϕ120 mm shaped charge.

The dimensional analysis results showed that when D = 148 mm, L_1 = 0.3 m, and L_2 = 5 m, then L_1/D = 2 and L_2/D = 33.8. This point is located on the curve in Figure 15. Specifically, the position of $P/D = f_1(L_1/D, L_2/D) = f_1(2,33.8)$ = 36.6 is marked in Figure 15. Hence, theoretically, the ϕ148 mm shaped charge could penetrate into the asphalt/soil/concrete composite target by 0.148 m × 36.6 = 5.417 m, including 0.3, 5, and 0.117 m of the asphalt, soil, and concrete parts, respectively. The relative error between the calculation and experimental results was 1.9%. When D = 120 mm, L_1 = 0.3 m, and L_2 = 3 m, namely, L_1/D = 3 and L_2/D = 25, the coordinates of this point in Figure 15 could be determined through the interpolation method as $P/D = f_1(L_1/D, L_2/D) = f_1(3,25) = f_1(2,25) + [f_1(2,25) - f_1(1.4,25)] \times (3-2) \div (2 - 1.4)$ = 34.7, and its position is marked in Figure 18. Therefore, theoretically, the ϕ120 mm shaped charge could penetrate into the asphalt/soil/concrete composite target by 0.12 m × 34.7 = 4.164 m, including 0.3, 3, and 0.864 m of the asphalt, soil, and concrete parts, and the relative error between the calculation and test results was 6.8%. The comparison between the test and calculated results is listed in the figure 19.

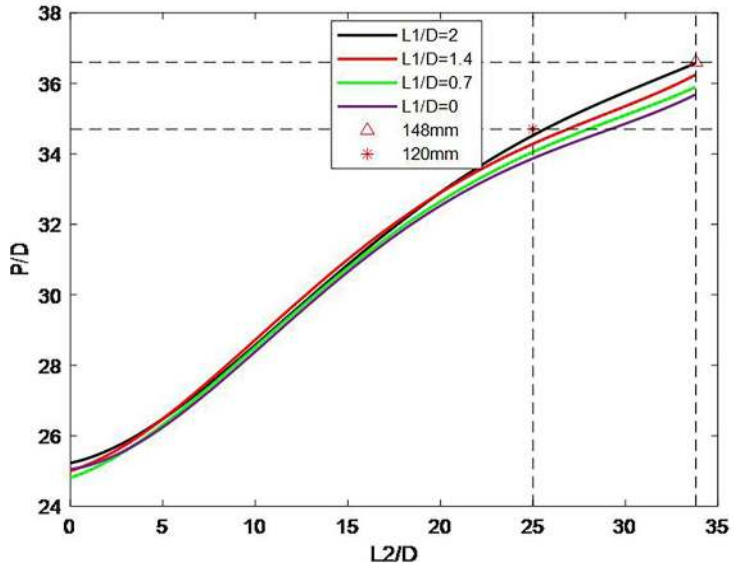

Figure 18 Experimental conditions.

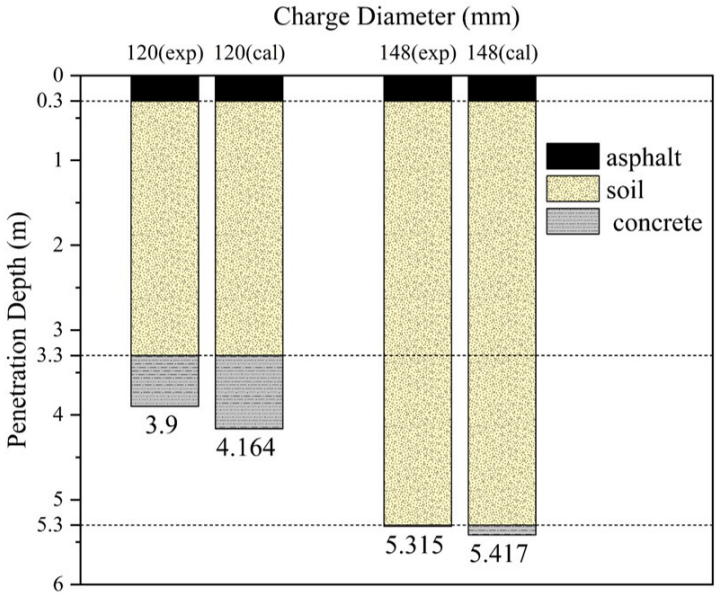

Figure 19 Comparison between experimental and calculated results in discussion.

5 Conclusion

In consideration of the influence of shock waves, jet fracture, and the interface effect, the calculation model for the penetration of shaped charge jets into asphalt/soil/concrete composite targets was established, jet formation was numerically simulated, and jet penetration performance was theoretically calculated. Moreover, the calculation results were verified by tests, and the diagram of the law governing the damage caused by jet penetration into media with differing thicknesses was obtained through dimensional analysis and theoretical modeling. Finally, the following conclusions were obtained:

(3) As a result of the interface effect, the shock waves generated when the shaped charge jet penetrates into the target plate are reflected and transmitted at the interface between two media. Under the action of reflected waves, the penetration velocity near the interface between different media declines, leading to the reduction in total penetration depth. Compression waves influence jet penetration performance more greatly than rarefaction waves.

(4) The penetration experiment was performed on an asphalt/soil/concrete composite target by using shaped charges. The results showed that the jet formed by the ϕ148 mm shaped charge could penetrate into the asphalt/soil/concrete composite target by 4.975 m, whereas that formed by the ϕ120 mm shaped charge could penetrate into the target plate by 4.3 m.

(5) The theoretical calculation and comparison with test results showed that the ϕ148 and ϕ 120 mm shaped charges could penetrate into the asphalt/soil/concrete composite target by 5.182 and 4.577 m, respectively, with relative errors of 4.2% and 6.4%, respectively. The test results are in good agreement with the theoretically calculated penetration depth.

(6) The relationships of total penetration depth with the changes in the thicknesses of the asphalt and soil parts were obtained through dimensional analysis and verified through two groups of experiments. The maximum relative error between the diagram of the damage law of jet penetration into media with differing thicknesses and test results was 6.8%, which could reflect the penetration depths of jets into different media with different thickness values.

Author's Contribuitions: Writing - original draft and Numerical simulation technical support, Yipu Dou; Writing - review & editing, Jianhao Dou and Zhengfeng Liang.

Editor: Pablo Andrés Muñoz Rojas

References

Baudin, G., Serradeill, R. (2010). Review of Jones-Wilkins-Lee equation of state. EPJ Web of Conferences 10: 00021. doi:10.1051/epjconf/20101000021.

Birkhoff, G., Macdougall, D. P., Pugh, E. M. and Taylor, S. G. (1948). Explosives with Lined Cavities. J. Appl. Phys. 19:563-582. doi: 10.1063/1.1698173.

Burakovsky, L., Preston, D. (2006). Shear modulus at all pressures: Generalized Guinan-Steinberg formula. J. Phys. Chem. Solids 67 (9): 1930-1936. doi:10.1016/j.jpcs.2006.05.041.

Chen, J., Liu, C., Dong, H., Shi, D., Zhang, Z. and Wang, D. (2013). Dynamic properties of concrete materials under shock loading. Construction and Building Materials 39: 119-123. doi:10.1016/j.conbuildmat.2012.05.011.

Chen, X., Li, Q. (2002). Deep penetration of a non-deformable projectile with different geometrical characteristics. Int. J. Impact Eng 27 (6): 619-637. doi:10.1016/S0734-743X(02)00005-2.

Chou, P., Flis, W. (1986). Recent Developments in Shaped Charge Technology. Propellants Explos. Pyrotech 11 (4): 99-114. doi:10.1002/prep.19860110402.

Chou, P. and Carleone, J. (1997). The stability of shaped-charge jets. J. Appl. Phys. 48: 4187–4195. doi: 10.1063/1.323456.

Church, P., Cornish, R. and Cullis, I. (2001). General overview of capability in the simulation of shaped charged charges penetration soil/concrete targets. In Proceedings of the 19th international symposium on ballistics, 1053-1060. Interlaken, Switzerland: TIBKAT.

Elshenawy, T., Elbeih, A. and Li, Q. (2018). Influence of target strength on the penetration depth of shaped charge jets into RHA targets. International Journal of Mechanical Sciences 136: 234-242. doi:10.1016/j.ijmecsci.2017.12.041.

Grady, d. (1996). Shock Equation of State Properties of Concrete. SAND-95-2215C; CONF-960774-1; ON: DE96006884, Sandia National Lab. (SNL-NM), Albuquerque, NM.

Guinan, M., Steinberg, D. (1975). A simple approach to extrapolating measured polycrystalline shear moduli to very high pressure. J. Phys. Chem. Solids 36 (7-8): 829. doi:10.1016/0022-3697(75)90109-2.

Held, M. (1983). Characterizing Shaped Charge Performance by Stand-Off Behavior, In Proceedings of the 7th International Symposium on Ballistics. The Hague, The Netherlands: TIBKAT.

Held, M. (1995). Verification of the Equation for Radical Crater Growth by Shaped Charge Jet Penetration. Int. J. Impact Eng 17 (1-3), 397-398. doi:10.1016/0734-743X(95)99864-N.

Held, M., Huang, N., Jiang, D. and Chang, C. (1996). Determination of the Crater Radius as a Function of Time of a Shaped Charge Jet that Penetrates Water. Propellants Explos. Pyrotech 21 (2): 64-69. doi:10.1002/prep.19960210203.

Held, M., Kozhushko, A. (1999). Radial Crater Growing Process in Different Material with Shaped Charge Jets. Propellants Explos. Pyrotech 24 (6): 339-342. doi:10.1002/(SICI)1521-4087(199912)24:6<339::AID-PREP339>3.0.CO;2-5

Jia, X., Huang, Z., Zu, X., Gu, X., Zhu, C. and Zhang, Z. (2013). Experiment study on the performance of woven fabric rubber composite armor subjected to shaped charge jet impact. Int. J. Impact Eng 57: 134-144. doi:10.1016/j.ijimpeng.2013.01.014.

Jia, X., Huang, Z., Zu, X., Gu, X. and Xiao, Q. (2014). Theoretical analysis of the disturbance of shaped charge jet penetrating a woven fabric rubber composite armor. Int. J. Impact Eng 65: 69-78. doi:10.1016/j.ijimpeng.2013.11.005.

Lee, E., Hornig, H. and Kury, J. (1968). Adiabatic expansion of high explosive detonation products. UCRL-50422, Univ. Of California Radiation Lab. at Livermore, Livermore, California, CA. doi:10.2172/4783904.

Leonga, E.C., Anand, S., Cheong, H.K. and Limb, C.H. (2007). Re-examination of peak stress and scaled distance due to ground shock. Int. J. Impact Eng 34 (9): 1487-1499. doi:10.1016/j.ijimpeng.2006.10.009.

Li, J., Zhang, Y. and Zhang, Z. (2023). Damage Effect Evaluation of Air-to-ground Missile on Airport Runway. Ordnance Industry Automation 42 (10): 4-7. (in Chinese)

Li, X., Zhang, D., Yang, Y. and Zhang, H. (2019). Simple analysis on main features and future development of urban operation. Protective Engineering 41: 64-68. (in Chinese)

Liu, J., Guo, X. Q., Liu, Z. J., Liu, X. and Liu, Q. Y. (2019). Pressure field investigation into oil&gas wellbore during perforating shaped charge explosion. Journal of Petroleum Science and Engineering 172:1235-1247. doi:10.1016/j.petrol.2018.09.068.

Liu, X. B., Li, J., Liu, G. H., Lian, W., Yang, H. W., Wang, D. and Liu, P. L. (2023). Analysis of FEM-SPH coupling for perforation penetration variation under different geology-engineering conditions. Computational Particle Mechanics 11: 867-883. doi:10.1007/s40571-023-00658-y.

Lu, Z., Sabatier, J. (2009). Effects of Soil Water Potential and Moisture Content on Sound Speed. Soil Science Society of America Journal 73 (5): 1614-1625. doi:10.2136/sssaj2008.0073.

Mamivand, M., Liaghat, G. (2010). A model for ballistic impact on multi-layer fabric targets. Int. J. Impact Eng 37 (7): 806-812. doi:10.1016/j.ijimpeng.2010.01.003

Meyers, M. (1994). Shock waves, in Dynamic Behavior of Materials. New York, US: John Wiley & Sons, Inc.

Segletes, S. (1983). Drift Velocity Computations for Shaped-Charge Jets. ARBRL-MR-03306, US Army Ballistic Research Laboratory. Aberdeen Proving Ground, MD, USA.

Shelton, R. and Arbuckle, A. (1979). A calculation of particle size distributions in the break-up of shaped charge jets. J. Appl. Phys. 50, 6190–6195. doi:10.1063/1.325751.

Szendrei, T. (1983). Analytical Model for Crater Formation by Jet Impact and Its Application on Penetration Curves and Profiles. In Proceedings of the 7th International Symposium on Ballistics, 575-583. The Hague, The Netherlands: TIBKAT.

Szendrei, T. (1995). Analytical Model for High-Velocity Impact Cratering with Material Strengths: Extension and Validation. In Proceedings of the 15th International Symposium on Ballistics, ed. M. Mayseless, and S. Bodner, 123-131. Jerusalem, Israel: TIBKAT.

Tan, Q. (2005). Basic Principles, in Dimensional Analysis. HeFei, China: University of Science and Technology of China Press. (in Chinese)

Xiao, Q., Huang, Z., Zhu, C. and Zu, X. (2013). Calculation of Depth and Crater Diameter for the Supersonic Penetration of Shaped Charge Jet into Concrete. Propellants Explos. Pyrotech 38 (2): 224-231. doi:10.1002/prep.201200065.

Xiao, Q., Huang, Z., Zu, X. and Jia, X. (2015). Influence of Drift Velocity and Distance Between Jet Particles on the Penetration Depth of Shaped Charges. Propellants Explos. Pyrotech 41 (1): 76-83. doi:10.1002/prep.201500051.

Xiao, Q., Huang, Z., Jia, X., Zu, X. and Zhu, Q. (2017). Shaped charge penetrator into soil-concrete double-layered target. Int. J. Impact Eng 109: 302-310. doi:10.1016/j.ijimpeng.2017.07.003.

Xiao, Q., Huang, Z., Zu, X., Jia, X., Zhu, Q. and Cai, W. (2020). Shaped charge penetration into high- and ultrahigh-strength Steel-Fiber reactive powder concrete targets. Defence Technology 16 (1): 217-224. doi:10.1016/j.dt.2019.04.013.

Yankelevsky, D.Z., Karinski, Y.S. and Feldgun, V.R. (2011). Re-examination of the shock wave's peak pressure attenuation in soils. Int. J. Impact Eng 38 (11): 864-8181. doi:10.1016/j.ijimpeng.2011.05.011

Zheng, Z. (1981). Stability of jet produced by shaped charge. Explosive and Shock 7: 6-17. (in Chinese)

Zhang, X. M., Zhou, X. S., Wang, L. C., Yang, G. F., Feng, H., Gao, X. and Ma, M. Z. (2020). Attenuation of blast wave in a large-section tunnel. Explosive and Shock Waves 40(2): 119-129. doi:10.11883/bzycj-2019-0045. (in Chinese)

Zu, X., Huang, Z., Xiao, Q. and Liu, B. (2015). Theoretical Study on Equivalent Target of Ceramic Composite Armor. Propellants Explos. Pyrotech 40 (4): 576-582. doi:10.1002/prep.201400186fig.